Predictive Modelling and Optimisation of Power Generation for the M4 Wave Energy Converter: A Deep Learning Approach

S. Hoekstra, D. Howe, A. Kurniawan

Abstract — This paper investigates the use of a nonlinear autoregression neural network for wave field predictions, and its implementation into a power-take off passive loading control system which tunes the damping coefficient for a wave energy converter. The wave energy converter considered in this study is a part of a multi-institutional demonstrator project which has seen the deployment of a moored multimodal multibody (M4) attenuator wave energy converter in King George Sound in Albany, Western Australia. The device consists of a 1-2-1 float configuration and is approximately 20 meters in length. The developed neural network was used to predict wave elevations and energy spectrums for 10-second and 20-second ahead of time intervals. Findings of this study show that the neural network was able to accurately predict up to 10 s intervals (where RMSE = 1.32E-02), however the accuracy of predictions fell for 20 s predictions (where RMSE = 5.20E-02). A linear numerical model of the prototype M4 device was used to find the optimal PTO damping coefficient for the observed wave fields at King George Sound. This allowed for optimisation of mean absorbed power for a generated 3-hour JONSWAP unidirectional timeseries using variable damping coefficients. Here, the power output was able to be increased by 106% for a significant wave height of 0.63 m and peak period of 3 s and resulted in an overall increase in capture width ratio across the 3-hour wave dataset.

Keywords— Wave Energy Converter, neural network, wave spectrum, power take-off.

Part of a special issue for ICOE 2024. Manuscript submitted 28 March 2025; Accepted 10 April 2025. Published 9 September 2025.

This is an open access article distributed under the terms of the Creative Commons Attribution 4.0 International license. CC BY https://creativecommons.org/licenses/by/4.0/. Unrestricted use (including commercial), distribution and reproduction is permitted provided that credit is given to the original author(s) of the work, including a URI or hyperlink to the work, this public license and a copyright notice. The authors acknowledge the financial support of the Blue Economy Cooperative Research Centre, established and supported under the Australian Government's Cooperative Research Centres Program, grant number CRC-20180101.

This article has been subject to a single-blind peer review by a minimum of two reviewers.

I. Introduction

ONCERNS regarding increasing energy demands and environmental impact from carbon dioxide emissions has seen an interest for the development of sustainable energy from renewable sources. With oceans covering 71% of the Earth's surface, there is large potential for wave energy to become a viable source of renewable energy. Swells on Australia's South-West coastline is predominantly large from uninterrupted weather systems migrating from the Southern Indian Ocean [1], resulting in significant wave energy potential. Furthermore, the ocean represents one of the world's largest unexplored sources of energy, with waves providing energetic features throughout the day and night and throughout the seasons. It is noted that waves could provide electricity up to 90% of the time, but wind and solar power systems may only create electricity 20-30% of the time [2]. Here, Wave Energy Converters are being researched and developed as a potential solution to these recent concerns. However, they are yet to become commercialised, and mass produced.

According to their working principle, WEC's can be classified into three main categories: (1) oscillating-body which utilise a float, buoy or pitching device to extract energy from waves, (2) oscillating water column (OWC) where wave motion causes air flow within a chamber subsequently driving a turbine, and (3) overtopping devices in which water overflows the device through hydraulic turbines. Various forms of WEC's have been previously explored, including the King Island Project

S. Hoekstra was at the Centre for Maritime Engineering and Hydrodynamics, Australian Maritime College, University of Tasmania, Locked Bag 1395, Launceston, Tasmania 7250, Australia. They are now at DOF Australia, 181 St Georges Terrace, Perth WA 6000 (e-mail: Samantha.hoekstra.4@gmail.com)

D. Howe is with the Centre for Maritime Engineering and Hydrodynamics, Australian Maritime College, University of Tasmania, Locked Bag 1395, Launceston, Tasmania 7250, Australia. They are also with the Blue Economy Cooperative Research Centre, Launceston, Tasmania 7250, Australia (e-mail: damon.howe@utas.edu.au).

A. Kurniawan is with Marine Energy Research Australia, The University of Western Australia, 35 Stirling Terrace, Albany, Western Australia 6330, Australia (e-mail: adi.kurniawan@uwa.edu.au).

Digital Object Identifier: https://doi.org/10.36688/imej.8.287-297

from Wave Swell Energy. This project saw the deployment of the UniWave200 at Grassy, King Island, Tasmania which successfully operated for 12 months. The device was an oscillating water column type, spanning 22.1 m in long 13.6 m wide and 14.2 m tall, and had a maximum output of 200 kW [3]. Although the project was successful, the large size and small power output highlights one of the problems which WEC's face for becoming viable for mass production commercialisation. This suggests that further research is needed to develop smaller WEC's units capable of harvesting higher levels of electricity from the ocean's waves. For a wave energy converter, typically the major costs are associated with foundations and moorings, structure, and maintenance and operations. Optimising the power capture allows for a lower number of required structures to achieve the desired power output and therefore reducing costs.

This paper sets out to investigate increasing the generated power output from a Moored Multimodal Multibody (M4) WEC through incorporating predictive modelling from a neural network into a PTO passive damping control system. Here, a nonlinear autoregressive neural network is used to predict oncoming wave elevation which produces an optimal rotational damping coefficient which correlates to the specific PTO system used within the device. The materials of this paper are set out as follows: Section II provides insight into the M4 WEC and applications of neural networks, Section III describes the methodology used within this paper, Section IV provides results and discussions.

II. BACKGROUND INFORMATION

A. M4 wave energy converter

The M4 WEC is of the attenuator type which is a part of a multi-institutional program funded by Blue Economy CRC and the Western Australian Government. The project aimed to deploy a demonstrator device in King George Sound, Albany, Western Australia. The device is approximately 20 m in length and consists of two framed rigid bodies, capturing energy through the relative motion of multiple floats in a 1-2-1 configuration, shown in Fig. 1. A triangular formation of the first three floats makes up the forward body where the final float is connected on the aft body via a hinge coupled with a PTO system. The floats are arranged in increasing diameter from forward to aft allowing the device to naturally weathervane from a single point mooring, aligning itself parallel to wave propagation direction. The WEC couples heave, surge, and pitch excitation to enhance energy capture by combining the principles of point absorber and hinge-raft converters [4]. The M4 design investigated in this study has been formed from previous studies which investigated design principle [5]. Initially, three rectangular floats were arranged longitudinally with equal distance of half a wavelength. Optimisation of the M4 device found that reducing the

drag coefficient of the three floats by introducing a rounded base increased the energy capture by up to 60% [6]. Furthermore, increasing the bow to mid float spacing to be more than the mid to stern float spacing found improvements to the energy capture [7]. A study explored the influence of increasing the number of floats from 3 to 8 in various configurations through a linear diffraction timedomain model which saw significant increase in energy capture [8]. However, considering the levelised cost of electricity (LCOE), the 6-float 1-3-2 and the 4-float 1-2-1 configurations were found to be more beneficial. Both of these configurations have been previously researched for energy yield in several sites. A study conducted by [9] compared the mean power output of a 3-float configuration in two potential sites: Albany, Western Australia and Orkney, United Kingdom. The power performance of the two sites were found to be similar, but the severity of extreme waves at Albany is considerably less and therefore more desirable from a survivability perspective.

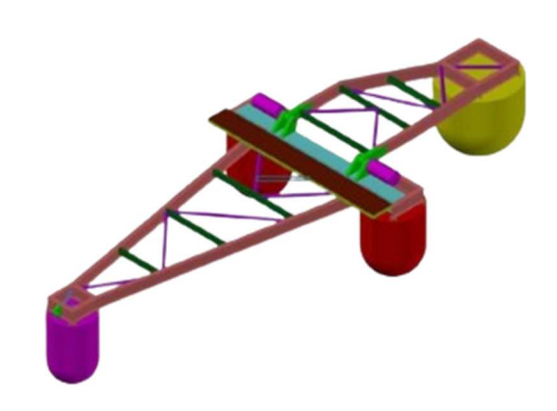


Fig. 1. 3D-schematic of the 1-2-1 M4 configuration showing increasing float diameter, excluding power take-off.

Further potential optimisation of the M4 device may include optimisation of the PTO system. The PTO for the M4 device includes an electrical drive train with a permanent magnet (PM) generator which allows for variable torque in the form of a damping coefficient in relation to wave conditions at site [10]. Wave climate is variable in nature, resulting in implications for WEC energy capture and the efficiency of the device. Here, it may be beneficial to implement a passive loading control system which tunes the PTO damping coefficient relative to the oncoming wave field, therefore optimising power generation for temporal wave fluctuations. For example, for rotational motion the passive loading control system will provide a given counter torque for a certain angular velocity. PTO control systems have been investigated previously on a heaving WEC by incorporating varying PTO damping through utilising the Sliding Discrete Fourier transform technique to estimate local wave frequency [11]. Here, the PTO damping was adjusted according to the estimated frequency. Results showed power capture increased from 1.64% to 10.38%. PTO optimisation of the 3-float configuration M4 device was

explored through incorporating a linear non-casusal controller for damping pitch control [12]. The study predicted the incoming sea state with a Kalman filter and used this information in the non-casusal controller to contribute to the controller's decision making. Numerical results showed that the power capture was dramatically increased with this technique. Other methods for predicting the incoming sea state used for PTO controls include neural networks. This was explored for a point absorber which used a multi-layer artificial neural network to forecast short-term wave forces [13], which saw an increased energy absorption of 60-80%.

B. Neural networks

Neural networks (NN's) work on the basis of the human brain where, in the simplest form, a series on nodes are connected in three layers (see Fig. 2): an input layer including initial data for the network, a hidden layer where the main computational processing occurs, and an output layer which processes results for the given input [14]. NNs are used to provide predictions based on the input training data sets. Various NNs have been developed for applications ranging from classification, speech recognition, timeseries prediction and system control. Types of NNs include Convolutional Neural Networks (CNN), Long Short-Term Memory (LSTM) networks, Deep Neural Network (DNN), and Recurrent Neural Networks (RNN) [15].

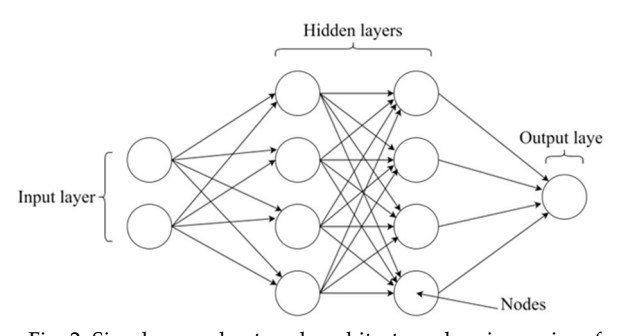


Fig. 2. Simple neural network architecture showing series of nodes connecting the input, hidden and output layers.

NNs have previously been used in the engineering industry to predict longitudinal-lateral dynamics of an autonomous vehicle [16]. Additionally, a developed DNN was used for time-varying multibody dynamic response of a crank shaft and connecting rod [17]. In WEC applications, the accuracy of predicting power generation was compared through different types of NNs [18]. The accuracy of NNs is partially dependent on network architecture hyperparameters such as batch size, epochs, and number of hidden layers. In the case of forecasting in the time-domain, both computational speed and accuracy of predictions play a critical role when forming hyperparameters of the NN. A previous study conducted a sensitivity analysis on the number of hidden layers with a range of neurons in each layer using the heave motion of a point absorber [19]. It was found that two hidden layers produced more accurate predictions compared to a single layer for the specified range of neurons. However, it was

found that the addition of the second hidden layer and neurons increased the computational processing time. Therefore, it is critical to find a balance between these parameters utilising NN hyperparameters.

C. Problem statement

Although sufficient research has been conducted on the M4 device and implementing PTO control systems on other forms of WECs to optimise power capture by forecasting the sea state, minimal research has been conducted on combining these by using a neural network to optimise the M4 device. Advantages of using a NN over other methods such as Kalman filter is that NNs can be complex with their number of layers and neurons and their parameters are learnt, whereas Kalman filter rely on a precise mathematical model of the system [20]. Therefore, a NN allows the control system to be flexible and be used in different locations on different WEC devices. The main scope of this study is to investigate the effects of a PTO damping control system on the M4 WEC by utilising a nonlinear autoregressive neural network to predict the oncoming wave elevation.

III. METHODOLOGY

D. Nonlinear Autoregressive Neural Networks (NARX)

Nonlinear Autoregressive (NAR) neural networks are a subclass of RNNs which are one of the well-known machine learning methods to model nonlinear dynamic systems. NAR is a time delay recurrent neural network which learns a series of patterns and nonlinear features based on feedback connections through different layers of the network [21]. It generally provides good multi-step forecasting in the short term. A modification of the NAR network is the NARX network which incorporates exogenous timeseries into the input training data. This exogenous timeseries is based on external data which has an impact on what the neural network is predicting. In the case of wave forecasting, this external data could be in the form of wind speed and directional data, tidal data, geographical features and historical wave data. The inclusion of the exogenous series is expected to provide improvements to the accuracy of predictions as these parameters can influence the wave climate. NARX networks are capable of making multistep ahead predictions in the time-domain, defined by (1) [22]. This is used for wave forecasting in this paper.

$$Y(t) = f(y(t-1), y(t-2), ..., y(t-n_d), u(t-1), u(t-2), ..., u(1-n_d))$$
(1)

where, f is the activation function, Y(t) is the predicted output sequence, y(t) is the input sequence, u(t) is the exogenous sequence and n_d is the specified time delay.

A typical NARX network consists of an input layer, one or more hidden layers and an output layer. The NARX network architecture used in this study included an open

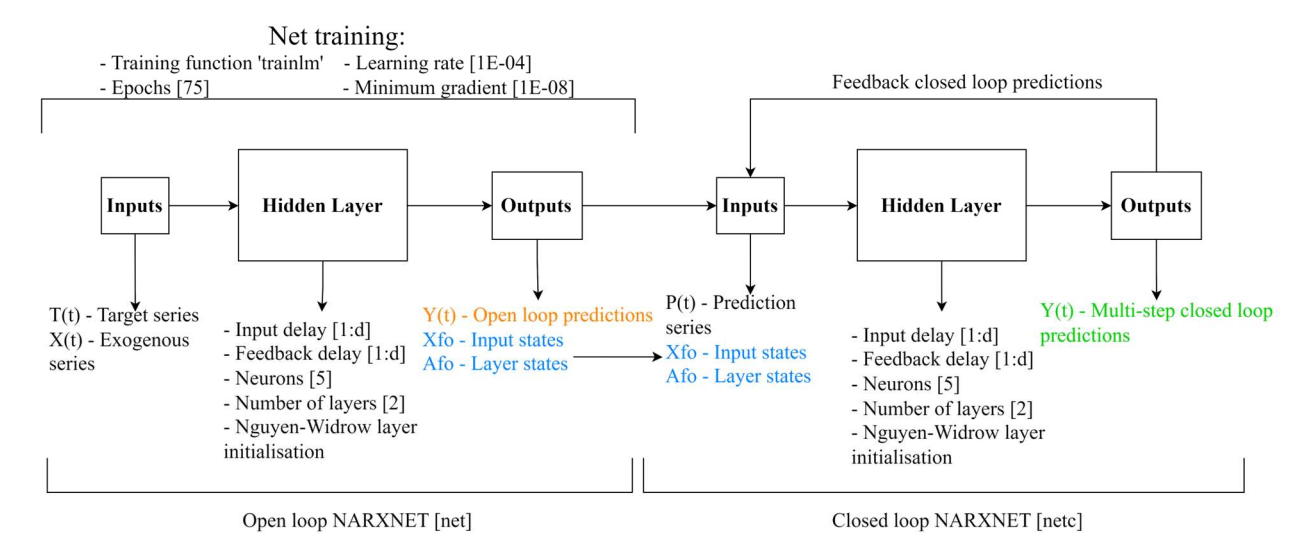


Fig. 3. Nonlinear autoregressive neural network architecture used in this study showing the defining parameters

loop used for network training and a closed loop used for predictions, as shown in Fig. 3. For the open loop, both the input and exogenous timeseries data were used to define initial weights and biases (input layer states). Here, no feedback connections are used forming an 'open loop'. The initial weights and biases were then used in a closed loop along with a predefined prediction timeseries to forecast successive timesteps. In the closed loop, feedback connections are used for dynamic output predictions which are then postprocessed via comparison to expected wave elevation values. The model is trained using the Levenberg-Marquardt backpropagation training function which updates weights and bias according to Levenberg-Marquardt optimisation as this has previously been defined as the fastest backpropagation algorithm [23]. In this study, the number of input and feedback time delays, wave sampling frequency, prediction time length and number of epochs were used as parameters for optimisation of the prediction performance.

E. Neural network performance evaluation

Three criteria, Mean Squared Error (MSE), Root Mean Squared Error (RMSE) and coefficient of determination (R²) are employed to evaluate the neural networks prediction performance. Values of MSE and RMSE close to zero and values of R² close to one show agreement between the true wave elevation and the model's predictions. These criteria are calculated below through (2), (3) and (4).

$$MSE = \frac{1}{n} \sum_{i=1}^{n} (y_i - \hat{y_i})^2$$
 (2)

$$RMSE = \sqrt{MSE} \tag{3}$$

$$R^2 = 1 - \frac{n \times MSE}{\sum_{i=1}^{n} (\gamma_i - \overline{\gamma}_i)}$$
 (4)

where, n is the number of observations, \hat{y}_i is the predicted values and \bar{y}_i is the mean of the true values.

F. Wave elevation data sets

Absorbed power of a WEC is related to the wave elevation and the PTO system. Therefore, the NN predicts wave elevation for a specified time interval from timeseries JONSWAP data correlating to what can be seen at King George Sound. Fig. 4(a) presents the bivariate probability distribution of significant wave height and mean period recorded from a Spotter wave buoy at the target location from January 2021 to January 2022. From this, the most predominant significant wave height of 0.625 m and mean period of 5.50 s were used to create synthetic unidirectional 3-hour JONSWAP timeseries data for the NN. As the target location is in shallow waters, the peak enhancement factor of the JONSWAP spectrum was 1. Fig. 4(b) represents the generated JONSWAP spectrum for the created wave timeseries.

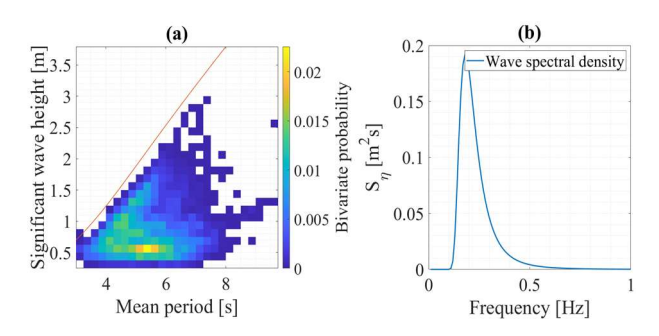


Fig. 4. (a) bivariate probability distribution of the significant wave height and mean period at King George Sound from January 2021 to January 2022; (b) Generated JONSWAP spectral density for a 3-hour irregular wave, gamma = 3.

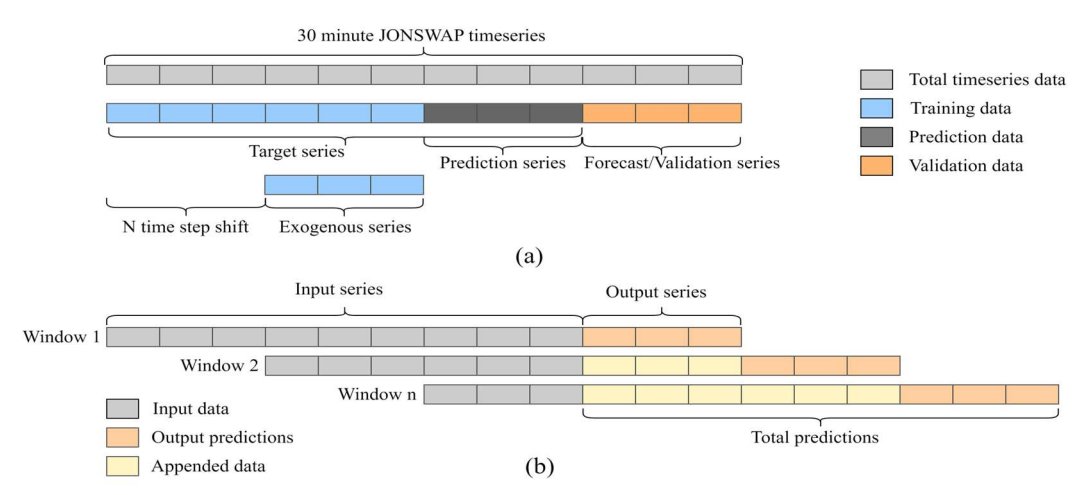


Fig. 5. (a) Data structure of NARXNET for singular 30-minute timeseries; (b) sliding window approach used for successive predictions for full 3-hour timeseries.

G. Data pre-processing

Pre-processing the timeseries data is an essential step when determining the inputs for the NN. It is essential to note that during the pre-processing process, the timeseries data is split into an initial 30-minute duration to save computational power and training time. This series was then further split into wave target and exogenous series, prediction series and validation series shown in Fig. 5(a). The data is split according to the number of time steps (*N*) required to predict a specified length of time. The target series, or training series, includes the portioned 30-minute wave elevation data from t = time(1, ...end - N). The exogenous series uses historical wave data. In the case of this study, the historical wave data is shifted back *N* time steps. The prediction series uses the last *N* values from the target series and the validation data uses the last *N* values from the 30-minute series. For successive predictions, a sliding window approach was implemented. In this case, the target series is updated containing the forecasted observations and shifted forward N time steps, as shown in Window 2 of Fig. 5(b). Then the NARXNET is re-trained with the new 30-minute timeseries, forecasting the next series of wave elevation. This process is repeated for the remaining 3-hour timeseries.

Fig. 6(a) shows the target series data used for open loop

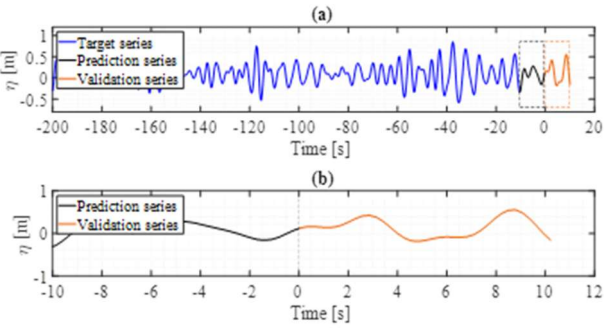


Fig. 6. (a) 30-minute JONSWAP scaled timeseries data used for NARXNET forecasting; (b) correlating scaled prediction series and validation series.

prediction series used in closed loop forecasting and the validation series. These can be seen in further detail in Fig. 6(b).

H. Numerical model

A numerical model of the M4 device was developed by Kurniawan et al. [24] which provides a linear, frequency-domain model based on the generalised mode approach. The model allows for the estimation of power, motions, relative freeboard, among other performance parameters to be computed. In this study, the linear power transfer function (see Fig. 7) was used to calculate the mean absorbed power for the wave spectrum. The 190 kNms/rad damping coefficient is representative of the full-scale model.

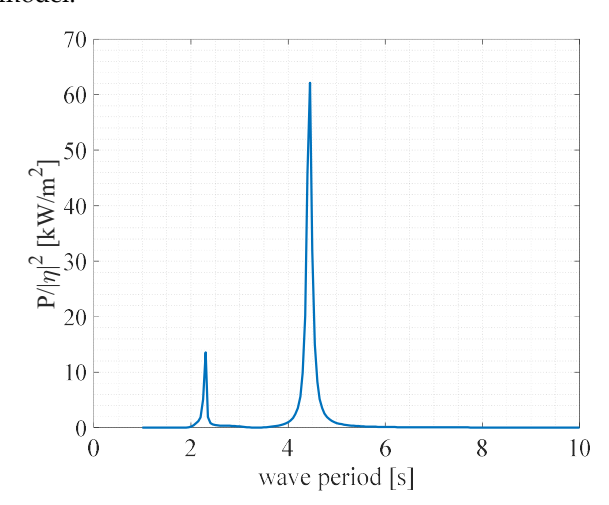


Fig. 7. Full-scale prototype M4 linear power transfer function with PTO damping coefficient of 190 kNms/rad.

I. Mean absorbed power and capture width ratio of WECs in irregular waves

For irregular waves, the mean absorbed power defined by an energy spectrum can be written as

$$P_c^{IRR} = \int_0^\infty 2S_{\eta}(f)P_c^{LTF}(f)df \tag{5}$$

training for the created wave. Additionally, it shows the

where, P_c^{LTF} is the linear power transfer function, and $S_n(f)$ is the energy spectrum of the irregular wave.

The mean incident wave power per unit width for a significant wave height H_s in irregular waves (assuming deep water) is written as

$$P_i^{IRR} = \frac{1}{16} \rho g H_s^2 c_{ge} \tag{6}$$

where c_{ge} is the group velocity corresponding to the energy period (T_e) , $c_{ge}=gT_e/4\pi$ in deep water. As described in [5], $T_e=0.78T_p$ for $\gamma=1.0$ and $T_e=0.84T_p$ for $\gamma=3.3$ with γ being the peak enhancement factor of the JONWAP spectrum.

The capture width ratio (CWR) indicates the power absorption capability of any WEC and is defined as

$$CWR = \frac{P_C^{IRR}}{P_I^{IRR}W} \tag{7}$$

where *W* is the device width perpendicular to wave propagation direction.

IV. RESULTS AND DISCUSSION

I. Prediction variables study

Sensitivity analysis is critical for the development of a neural network in determining parameters which will provide accurate results. This was conducted to evaluate the effects of important input variables on the accuracy of the network predictions and the required computational time. In this case, such parameters included the time delay, prediction length, sample frequency, and number of epochs.

1) Effect of time delay and prediction length

A sensitivity study was conducted on the input and feedback time delay to determine the ideal number of time steps which are fed into each iteration of training for accurate wave field predictions, whilst minimising processing computational duration. As a forecasting method for PTO damping control, it is critical that the computational duration is less than the prediction time frame. Optimising the delay requires a good balance between computational duration and accuracy while avoiding overfitting and underfitting the data. Large delays result in overfit data with large computational processing. For this sensitivity analysis, two prediction time lengths were studied of a 10 s and 20 s duration for a significant wave height of 0.625 m and peak period of 5.50

Error metrics such as MSE, RMSE and R² were used to test the accuracy for each time delay and prediction length. Table I details the sensitivity analysis for a 10 s prediction length where the error metrics correspond to the wave elevation predictions. It can be noted that increasing the delay increases the accuracy of predictions, as increasing the delay increases the number of previous time-steps that the network considers when making future predictions. A

Table I NN delay sensitivity analysis with a prediction length of 10 s $(N=36), H_{\rm S}=0.625~{\rm M}~{\rm And}~T_{\rm P}=5.5~{\rm s}.$

Delay	Computational	MSE	RMSE	\mathbb{R}^2
	time [s]			[%]
10	1	8.87E-03	9.41E-02	37.91
20	2	3.31E-03	5.74E-02	76.86
30	4	3.08E-03	5.55E-02	78.46
40	6	2.20E-03	4.69E-02	84.59
N+10	7	4.79E-04	2.19E-02	96.65

Table II NN delay sensitivity analysis with a prediction length of 20 s $(N=72), H_{\rm S}=0.625~{\rm M}~{\rm And}~T_{\rm P}=5.5~{\rm s}.$

Delay	Computational	MSE	RMSE	R ² [%]
	time [s]			
30	4	1.35E-02	1.16E-01	-29.26
40	6	8.52E-03	9.23E-02	18.32
50	7	3.39E-03	5.82E-02	67.51
60	11	8.66E-03	9.31E-02	16.92
N+20	22	1.80E-03	4.25E-02	82.71

delay of the prediction time steps (N) plus 10 provided good correlation between predictions and validation data whilst computational duration remains less than the prediction length. Table II details the sensitivity analysis for a duration of 20 s. The N+20 delay depicts good accuracy; however, the computational duration is larger than the prediction time which introduces accumulating lag in long term predictions. Due to this, the NN predicts up to 10 s maximum with a delay of N+10.

2) Effect of sampling frequency

A sensitivity analysis was performed on the sampling frequency of the wave timeseries data to explore the effects on accuracy and computational duration from variability in the number of data timesteps (see Table III). The quantity of data used in training and predictions can affect the accuracy and training time of NNs as large data sets require much more processing capabilities. This analysis was conducted on the predominant 30-minute wave timeseries with sampling frequencies ranging from 3.5 Hz to 7.8 Hz. It can be noted that only the smallest sample frequency required less processing time than prediction length. Additionally, the accuracy of predictions decreases with increased sample frequency. However, this further increases the processing time. In this case, a sample frequency of 3.5 Hz was used throughout the rest of this study.

Table III $NN \mbox{ sample frequency sensitivity analysis with H_s = 0.625 m and } \\ T_P = 5.5 \mbox{ s, and prediction length of 10 s.}$

Sample frequency [Hz]	Computational time [s]	MSE	RMSE	R ² [%]
3.54	7	1.93E-04	1.39E-02	98.65
4.95	13	3.53E-04	1.88E-02	90.59
6.36	25	7.11E-03	8.43E-02	54.07
7.78	49	7.64E-03	9.04E-02	45.99

3) Effect of NN parameters

The effects of training epochs on neural network accuracy were also analysed. Epochs is a hyperparameter of neural networks which defines the number of times the learning algorithm works through the training series. The quantity of epochs used affects the accuracy and training time, as too large of a number may increase the computational duration with little gain in accuracy. The epoch sensitivity analysis was conducted for number of epochs from 25 to 100 in 25 increments. The number of hidden neurons was constant at 5 and the generated wave timeseries was used for each run. Table V details the resulting error metrics for each run. As the number of epochs increases, it can clearly be noted from Table V that

 $TABLE~V \\ NN~epoch~sensitivity~analysis~with~H_s=0.625~m~and~T_P=5.5~s, \\ and~prediction~length~of~10~s.$

Epochs	Computational time [s]	MSE	RMSE	R ² [%]
25	2	2.67E-03	5.16E-02	76.12
50	4	1.09E-03	4.36E-02	82.99
75	5	5.73E-04	2.39E-02	94.88
100	7	6.66E-04	2.58E-02	94.03

the accuracy converges at 75 whilst retaining a training time less than the prediction length.

K. Neural network predictions

A non-linear autoregressive NN was selected for this study because of its flexibility and capability of handling complex timeseries data. The NARX NN allows for quicker processing and training times compared to other NNs such as LSTMs. Upon creation and hyperparameter fine tuning of the NN, the wave elevation for 10 s and 20 s intervals were predicted for the generated JONSWAP spectrum. Although correlation of true and predicted wave elevation is important for showing the accuracy of the NN, the predictions of the corresponding energy spectrum is the critical parameter for determining the mean absorbed power when following (5). This means that the accuracy of the energy spectrum predictions is far more important in the application of this study. The error metrics for both 10 s and 20 s prediction intervals are detailed in Table IV. These were trained with a delay of *N*+10 and epochs of 75 for each interval with training times of 5 s and 16 s. When comparing the error metrics for wave elevation predictions to energy spectrum predictions, the neural network can predict the energy spectrum more accurately. Although the 20 s prediction interval was deemed unfeasible due to processing times being longer than prediction times, the accuracy of the energy spectrum for 20 s interval and a delay of N+10 shows promising results for the NN being capable of predicting longer time frames with further hyperparameter tuning. However, careful consideration must go into ensuring the training time is less than the prediction time. Fig. 8 analyses the wave elevation predictions for the 10 s interval where the

Table IV $Error\ metrics\ for\ 10\ s\ and\ 20\ s\ prediction\ lengths\ for\ the \\ Generated\ wave\ timeseries.$

	Prediction	MSE	RMSE	R ² [%]
	length [s]			
Time domain	10	1.75E-04	1.32E-02	98.77
analysis	20	2.71E-03	5.20E-02	74.00
Spectral domain	10	5.45E-08	2.34E-04	99.22
analysis	20	8.06E-07	8.98E-04	84.95

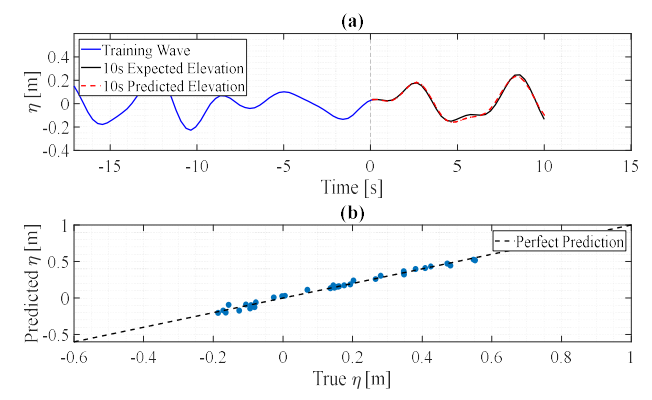


Fig. 8. (a) 10 s wave elevation prediction using the first 30-minute data set; (b) the 10 s predicted wave elevation against the true wave elevation

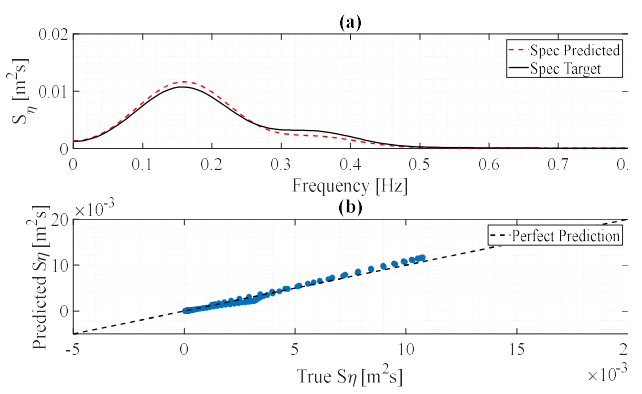


Fig. 9. (a) corresponding energy spectrum for validation and prediction data for 10 s interval; (b) validation energy spectrum against true energy spectrum.

corresponding energy spectrum predictions are detailed in Fig. 9. Additionally, the 20 s wave elevation predictions can be found in Fig. 10 with corresponding energy spectrums in Fig. 11.

In addition to the error metrics, the accuracy of the 10 s predictions was evaluated through comparing the predicted data to the true data in Fig. 8(b) and Fig. 9(b) via providing a visual representation where the linear regression line indicates a perfect prediction. Taking note of Fig. 9(a), an observable deviation in the height of the predicted energy spectrum peak shows the NN slightly over predicts the energy spectrum. This deviation is the resultant of the small inaccuracies between wave elevations in Fig. 8(a). Although the error metrics show the energy spectrum has more correlation between true and predicted values, the small deviation in peak heights can result in approximately 30% difference in mean absorbed power. Because of this, it is critical to ensure high accuracy in energy spectrum predictions.

Fig. 10 (a) Illustrates the predicted timeseries for 20 s. It can be noted that after approximately 10 s, the accuracy of wave elevation predictions decreases as shown in Fig. 10(b). Much like the 10 s prediction, the error metrics for the energy spectrum shows more accurate predictions compared to wave elevation as per Table IV. However, there are big differences between energy spectrum peaks in Fig. 11(a), which have an impact on the calculated absorbed power.

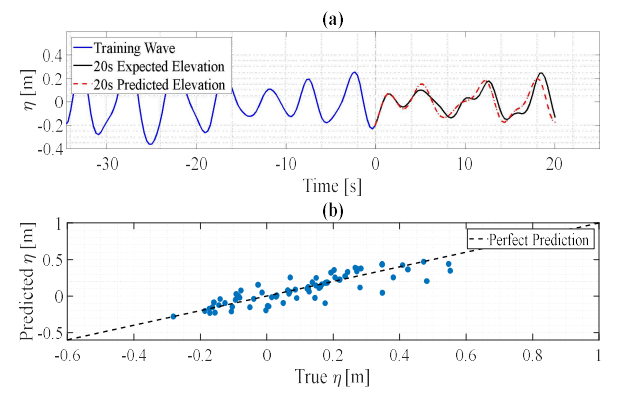


Fig. 10. (a) 20 s wave elevation prediction using the first 30-minute data set; (b) the 20 s predicted wave elevation against the true wave elevation.

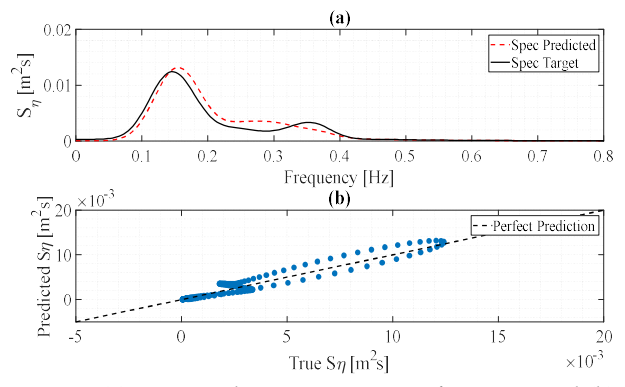


Fig. 11. (a) corresponding energy spectrum for $20\,\mathrm{s}$ interval; (b) validation energy spectrum against true energy spectrum.

L. Optimised PTO damping

The PTO damping coefficient is significant to the power absorption of WECs. The M4's damping coefficient is assumed to be a linear rotational damping type measured through the correlation between PTO torque and angular velocity. To provide insight into the dependence of optimised damping coefficients and the maximum power output, a comparison is made on the linear power transfer function for three damping coefficients (see Fig. 12). Referring to (5), a relationship can be formed between the optimal damping coefficient and the peak wave period of the energy spectrum. Although increasing the damping coefficient reduces the height of the peak frequency, it increases the bandwidth of all other peaks. This can be ideal for peak wave periods outside of the 3.5 s - 5 s range increasing the mean absorbed power. The optimal damping coefficient which provides the maximum power was calculated for the wave field at King George Sound, as seen in Fig. 13. Here, a peak period range between 3.5 s and 5 s requires the smallest damping coefficient from falling

within the bandwidth of the maximum peak of the transfer function. Anything which lies outside of this range gradually increases either side. This optimal damping coefficient is calculated solely on the maximum absorbed power and does not consider the limitations of real-time passive loading control which requires power from the device. Upon prediction of the wave elevation through the NARXNET, these optimised damping values were used along with their corresponding transfer function to calculate the mean absorbed power for the prediction time length.

M. Optimised mean absorbed power

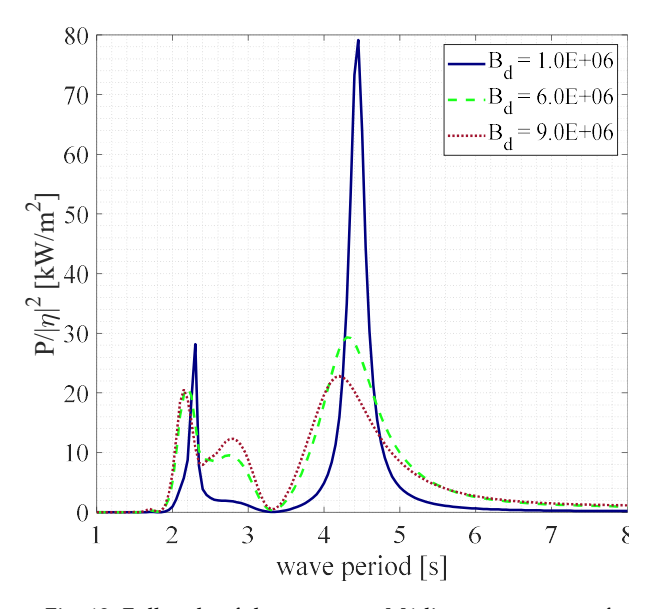


Fig. 12. Full-scale of the prototype M4 linear power transfer function showing effects of different PTO damping coefficients.

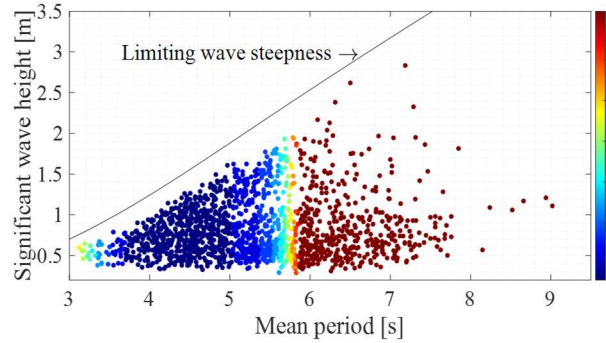


Fig. 13. Optimised PTO damping coefficient for the entire wave field at King George Sound.

Maximising the mean absorbed power for a WEC is critical to the potential commercialisation of these types of devices as it increases economic viability from requiring fewer devices to operate, further reducing the environmental impact from reduced footprint in the ocean. Using the sliding window approach, variable damping optimisation and therefore power output was implemented to each predicted 10 s interval. This was completed for the entire 3-hour generated wave timeseries with significant wave height of 0.625 m and peak period of 3 s.

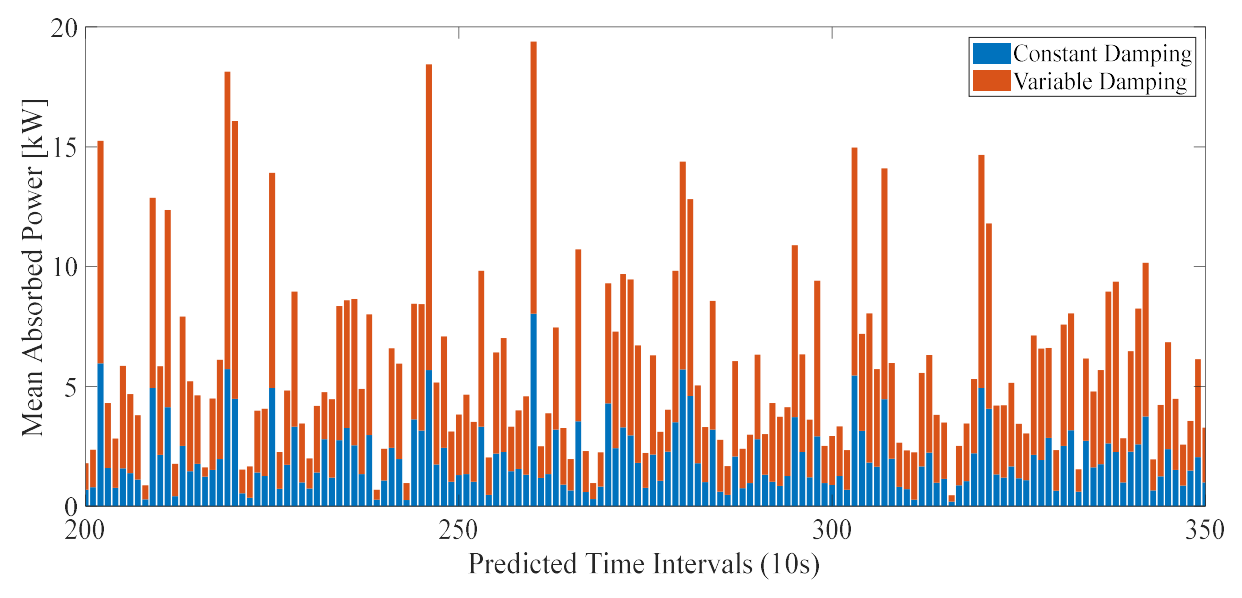


Fig. 14. Comparison between mean absorbed power for constant and variable damping coefficients for each 10s predicted intervals from three-hour wave input.

Fig. 14 details 25-minutes of predicted 10 s intervals using the NN and the corresponding optimised power output, showing a large increase in comparison to a constant damping coefficient of 190 kNms/rad. The corresponding power output and CWR for the two conditions can be found in Table VI. It can be noted the power output doubles by introducing a variable damping control system. However, this only represents one

 $TABLE\ VI$ Effects of variable damping compared to constant damping on the mean absorbed power and CWR for the generated 3-hour wave.

Damping type	Mean absorbed power	CWR
Constant damping	2.37 kW	64.8%
Variable damping	4.68 kW	127.7%

significant wave height and peak period.

Further analysis was completed on the CWR over a longer duration to capture more accurately the change in CWR for different wave fields. This included calculating the CWR for different 3-hour JONSWAP wave timeseries with peak periods from 2.5 s to 6 s and a significant wave height of 0.625 m. With variable PTO damping coefficients, the expected increase in CWR for the time-domain can be seen in Fig. 15. The M4 prototype WEC has a natural hinge rotation frequency of 3.142 seconds which corresponds to the maximum CWR of 1.4 for variable damping at a 3 second peak period. On average, the CWR was able to be increased by 147.4%.

The increase in CWR highlights the advantages of implementing a variable PTO damping control system for WECs as a higher CWR indicates larger power capture of the device. This can be beneficial for WEC co-location with offshore developments such as aquaculture. More significant WEC power capture decreases the reliance on diesel generators. For implications involving powering

other developments such as onshore housing, greater power capture of a single device results in requiring smaller scale of structures which decreases

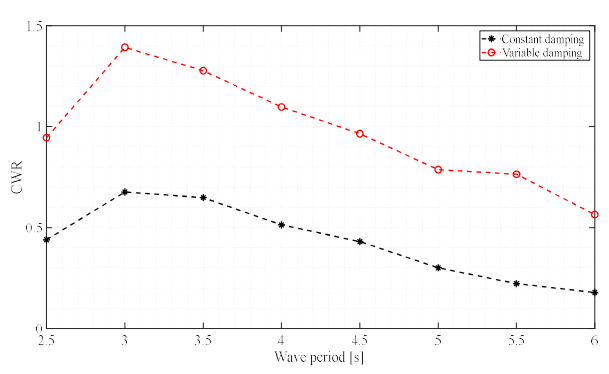


Fig. 15. Capture width ratio for constant damping coefficient of Bd = 190 kNms/rad and variable damping coefficients.

foundations/moorings and maintenance, therefore reducing costs.

V. LIMITATIONS AND FUTURE WORKS

Although the constructed neural network architecture predicts 10 s wave elevation intervals accurately, these short-term predictions may not be ideal from a mechanical perspective. Requiring the PTO control system to change the damping coefficient every 10 seconds puts unnecessary strain on the device, possibly resulting in further power losses. The integrated PTO system on the M4 device is a hydrodynamic-electrical model where the reference torque from the generator is fed back through a gearbox to the platform. In this case, the linear rotational damping coefficient would be varied by introducing a counter torque. Although an electrical PTO control system works much faster than a hydraulic system, implementing this counter torque every 10 seconds may introduce additional mechanical strain on the gearbox and require

additional power. For the PTO control system to be mechanically viable, the damping should vary in intervals of at least 30 seconds. However, this extended prediction length drastically decreases the accuracy of the neural network's predictions. To become mechanically viable and predict larger time intervals requires further NN hyperparameter fine tuning. Here, the time and feedback delay can be increased to help improve the accuracy of larger predictions. However, this may result in overfitting the data and excessive computational processing durations. All processing for this study was completed on a laptop with a CORE I7 processor. Upgrades on computational power can help mitigate the processing times and allow for larger prediction lengths. Furthermore, the robustness of the NN model can be increased via exploration of the exogenous data sets. In this study, wind data relevant to the wave field was not available. The inclusion of this in the exogenous data set may increase the accuracy of predictions and allow for longer prediction periods. Additionally, the model should be compared to other forms of neural networks such as a LSTM. This network is a type of recurrent NN designed to handle sequences of data. They are effective for timeseries forecasting and can capture long-term dependencies in the data, therefore may provide accurate predictions for wave elevation.

The generated wave time series included a unidirectional JONSWAP wave. However, this cannot accurately represent real-life ocean waves as directional spreading is generally prominent. Future work from this study should include analysing the accuracy of the NN for directional spreading in the wave field.

VI. CONCLUSIONS

This paper presents the investigation of utilising a neural network to predict oncoming wave elevation of unidirectional JONSWAP irregular waves. The predicted wave elevation and spectrum were implemented into a variable PTO damping system to increase the mean absorbed power of the M4 WEC prototype device which will be deployed in King George Sound in Albany, Western Australia. This study used a nonlinear autoregressive neural network with exogenous inputs to predict the wave elevation for 10 s and 20 s intervals. A sensitivity analysis was conducted on network hyperparameters such as number of input and feedback delay, prediction length, wave sampling frequency and number of epochs. It was found that the optimal prediction length for the architecture was no greater than 10 seconds with a delay of N+10, sampling frequency of 3.5 Hz and 75 training epochs. For prediction lengths greater than 10 seconds, it was found that the processing time surpassed the prediction length, therefore cannot be used in real-life applications.

Using the predetermined network hyperparameters from the sensitivity analysis, the energy spectrums were deemed more accurate compared to the predicted wave elevations with R² values of 99.22% and 98.77% respectively for the 10 s interval. However, the small variability in true and predicted energy spectrum peaks proved to have large implications on the absorbed power. Due to this, it was deemed critical to ensure that the accuracy of predictions for wave spectrums was to an excellent standard. A sliding window approach was used to predict the incoming wave elevation for the generated 3-hour timeseries in 10 s intervals. Here, variable damping coefficients were used to increase the absorbed power and CWR by an average of 147.4%. This is beneficial for WEC co-locations with offshore developments and when powering housing as the increased power capture allows for reduced reliance on diesel generators and less marine footprint therefore reducing costs.

ACKNOWLEDGEMENTS

The authors acknowledge the financial support of the Blue Economy Cooperative Research Centre, established and supported under the Australian Government's Cooperative Research Centres Program, grant number CRC-20180101. This work was developed as part of project 3.21.004 Seeding Marine Innovation in WA with a Wave Energy Deployment in Albany.

REFERENCES

- [1] M. A. Hemer and D. A. Griffin, "The Wave Energy Resource Along Australia's Southern Margin," Journal of Renewable and Sustainable Energy, pp. 2, 043108, 2010.
- [2] Arnob Barua and Md. Salauddin Rasel, "Advantages and challenges in ocean wave energy harvesting," Sustainable Energy Technologies and Assessments, Volume 61, 2024, 103599, ISSN 2213-1388, https://doi.org/10.1016/j.seta.2023.103599.
- [3] "King Island project WSE," WSE, Dec. 03, 2023. https://www.waveswell.com/king-island-project-2/ (accessed Jun. 18, 2024).
- [4] D. Howe, B. J. Raju, C. L. Hansen, H. Wolgamot, A. Kurniawan, J.-R. Nader, C. Shearer, and P. Stansby, "Basin testing of the 1-2-1 M4 WEC," in European Wave and Tidal Energy Conf., Bilbao, Spail, 7 2023.
- [5] P. Stansby, E. Carpintero Moreno, T. Stallard and A. Maggi, "Three-float broad-band resonant line absorber with surge for wave energy conversion," Renewable Energy 78, pp. 132-140, 2015.
- [6] P. Stansby, E. Carpintero Moreno and T. Stallard, "Capture width of the three-float multi-mode multi-resonance broadband wave energy line absorber M4 from laboratory studies with irregular waves of different spectral shape and directional spread," Journal of Ocean Engineering and Marine Energy, pp. 287-298, 2015.
- [7] P. K. Stansby, E. Carpintero Moreno and T. Stallard, "Modelling of the 3-float WEC M4 with nonlinear PTO options and longer bow beam," Renewable Energies Offshore: Proceedings of 2nd International Conference on Renewable Energies Offshore, pp. 263-268, October 2016.
- [8] P. Stansby, E. C. Moreno and T. Stallard, "Large capacity multifloat configurations for the wave energy converter M4 using a time-domain linear diffraction model," Applied Ocean Research: Volume 68, pp. 53-64, 2017.
- [9] H. Santo, P. Taylor and P. Stansby, "The performance of the three-float M4 wave energy converter off Albany, on the south coast of Western Australia, compared to Orkney (EMEC) in the U.K.," Renewable Energy: Volume 146, pp. 444-459, 2020.

- [10] J. M. Apsley, X. Zhang, I. Damian, M. Iacchetti, Z. Liao, P. Stansby, G. Li, G. Li, H. Wolgamot, C. Gaudin, A. Kurniawan, X. Zhang, Z. Lin, N. Fernando, C. Shearer and B. Saunders, "Integrated hydrodynamic-electrical hardware model for wave energy conversion with M4 ocean demostrator," Proceedings of the 15th European Wave and Tidal Energy Conference, 2023.
- [11] A. Burgac and H. Yavuz, "Power capture performance of a heaving wave energy converter for varying brad/bpto ratio," SN Applied Sciences, p. Article number: 1679, 2020.
- [12] Z. Liao , P. Stansby and G. Li , "Energy-maximizing control of pitch type wave energy converter M4," in American Control Conference (ACC), Philadelphia, 2019.
- [13] L. Li, Z. Yuan and Y. Gao, "Maximization of energy absorption for a wave energy converter using the deep machine learning," Energy 165(A), pp. 340-349, 2018.
- [14] G. Ognjanovski, "Everything you need to know about Neural Networks and Backpropagation Machine Learning Easy and Fun," 15 January 2019. [Online]. Available: https://towardsdatascience.com/everything-you-need-to-know-about-neural-networks-and-backpropagation-machine-learning-made-easy-e5285bc2be3a.
- [15] towardsAI, "Main Types of Neural Networks and its Applications — Tutorial," Towards AI, 13 07 2020. [Online]. Available: https://towardsai.net/p/machine-learning/main-types-of-neural-networks-and-its-applications-tutorial-734480d7ec8e. [Accessed 13 09 2023].
- [16] X. Nie, C. Min, Y. Pan, K. Li and Z. Li, "Deep-Neural-Network-Based Modelling of Longitudinal-Lateral Dynamics to Predict the Vehicle States for Autonomous Driving," Perception Sensors for Road Applications 22(5), 2022.
- [17] H.-S. Choi, J. An, S. Han, J.-G. Kim, J.-Y. Jung, J. Choi, G. Orzechowski, A. Mikkola and J. H. Choi, "Data-driven

- simulation for general-purpose multibody dynamics using Deep Neural Networks," Multibody System Dynamics (51), pp. 419-454, 2021.
- [18] C. Ni and X. Ma, "Prediction of Wave Power Generation Using a Convolutional Neural Network with Multiple Inputs," Energies, Vol. 11, no. 8, 2018.
- [19] S. Negulan, J. Selvaraj, A. Arunachalam and K. Sivanandam, "Performance of artificial neural network in prediction of heave displacement for non-buoyant type wave energy converter," IET Renewable Power Generation, pp. 81-84, 2016.
- [20] S. Feng, X. Li, S. Zhang, Z. Jian, H. Duan and Z. Wang, "A review: state estimation based on hybrid models of Kalman filter and neural network," Systems Science & Control Engineering, vol. Volume 11, no. 1, 2022.
- [21] K. Mahmoodi, E. Nepomuceno and A. Razminia, "Wave excitation force forecasting using neural networks," Energy Volume 247, p. 123322, 2022.
- [22] MathWorks, "Design Time Series NARX Feedback Neural Networks," 2023. [Online]. Available: https://au.mathworks.com/help/deeplearning/ug/design-time-series-narx-feedback-neural-networks.html.
- [23] M. T. Hagan and M. B. Menhaj, "Training feedforward networks with the Marquardt algorithm," IEE, vol. 5, no. 6, pp. 989-993, 1994
- [24] A. Kurniawan, H. Wolgamot, C. Gaudin, C. Shearer, P. Stansby and B. Saunders, "Numerical Modeling in the Development of the M4 Prototype for Albany, Western Australia," Proceedings of the ASME 2023 42nd International Conference on Ocean, Offshore and Arctic Engineering, no. 105185, 2023.